RSC Advances

PAPER

View Article Online
View Journal | View Issue

Cite this: *RSC Adv.*, 2025, **15**, 46496

Performance and mechanism of sulfamethoxazole degradation on a Magnéli-phase Ti_4O_7 reactive electrochemical membrane

Qiang Liu,[a] Yinuo Wang,[ab] Boxuan Yang, *[b] Jinwei Li, [b] Chengchun Jiang[b] and Huan Wang[b]

Antibiotics have emerged as a new class of environmental contaminants of global concern due to their persistence and potential ecotoxicological impacts. In order to enhance antibiotic removal efficiency, it is necessary to develop cost-effective and environmentally friendly wastewater treatment technologies. Magnéli-phase titanium oxide (Ti_4O_7) presents a promising solution, combining excellent metallic-like conductivity with ceramic-like corrosion resistance. In this study, the electrochemical oxidation of sulfamethoxazole (**SMX**) with a Ti_4O_7 reactive electrochemical membrane (REM) as the anode and stainless steel as the cathode was systematically investigated. The effects of key operational parameters, including current density, initial pH, supporting electrolyte type and concentration, and the presence of humic acid (HA) on **SMX** degradation were evaluated. Under optimal conditions (current density of 0.08 mA cm^{-2}, pH of 7, supporting electrolyte of 0.1 mol L^{-1} Na_2SO_4, no HA effect, and pump circulation), 99.7% **SMX** degradation was achieved within 2 hours. Quenching experiments and electron paramagnetic resonance (EPR) analysis confirmed that hydroxyl radicals (•OH) played a dominant role in **SMX** degradation. High-performance liquid chromatography coupled with quadrupole time-of-flight tandem mass spectrometry (HPLC-Q-TOF-MS/MS) identified key degradation intermediates, revealing three primary **SMX** degradation pathways: (1) •OH-mediated amino group oxidation, (2) S–N bond cleavage, and (3) $-NH_2$ hydroxylation. Additionally, Ecological Structure Activity Relationships (ECOSAR) software analysis demonstrated a significant reduction in overall toxicity following Ti_4O_7 oxidation. In summary, the Ti_4O_7 REM exhibits exceptional oxidation efficiency with low energy consumption, demonstrating strong practical feasibility and promising application potential for antibiotic-contaminated wastewater treatment.

Received 23rd August 2025
Accepted 18th November 2025

DOI: 10.1039/d5ra06264k

rsc.li/rsc-advances

1 Introduction

The frequent use of antibiotics and the low removal efficiency of traditional wastewater treatment plants for antibiotics have led to their gradual accumulation in natural water bodies, which poses a threat to human health by inducing antibiotic resistance.[1,2] Therefore, it is urgent to treat antibiotics to ensure their removal before discharging into natural water bodies. Among numerous antibiotics, sulfonamide drugs are widely used in human and veterinary medicine due to their broad-spectrum antibacterial activity, and sulfamethoxazole (**SMX**) is the most frequently detected substance in wastewater.[3] **SMX** exhibits high biological activity, strong bioaccumulation, difficulty in degradation, and low removal efficiency, posing significant health risks to humans, livestock, and plants.

The traditional wastewater and drinking water treatment systems exhibit poor removal efficiency of **SMX**.[4,5] Therefore, previous studies have mainly focused on enhancing **SMX** removal by using methods such as chemical oxidation,[6] advanced oxidation processes (AOPs),[7–9] photodegradation,[10] and reverse osmosis.[11] Although these methods indicate effective removal of **SMX**, some limitations and shortcomings still exist. For example, ozone oxidation demonstrates effective removal of **SMX**, but shows ineffective mineralization, and requires high investment costs and high ozone dosages. AOPs require continuous oxidants and catalysts for the degradation of wastewater, resulting in high operating costs and complex operations. In reverse osmosis, the membrane has a short lifespan and requires the addition of salt solution for further treatment, which is a complex and expensive operation.

Electrochemical advanced oxidation processes (EAOPs),[12,13] as an effective water and wastewater treatment technology, have been extensively researched and developed due to their versatility, non-selectivity, environmental acceptability, safety, and high energy efficiency.[14] Among numerous EAOPs, anodic

[a]*School of Municipal and Environmental Engineering, Shenyang Jianzhu University, Shenyang 110168, China*
[b]*School of Materials and Environmental Engineering, Shenzhen Polytechnic University, Shenzhen 518055, China. E-mail: yangboxuan@szpu.edu.cn*

oxidation (AO) is the most commonly studied, and pollutants can be removed by direct electron transfer (direct oxidation) or by generating active species *in situ* (indirect oxidation), such as hydroxyl radicals ($^{\bullet}OH$), hydrogen peroxide (H_2O_2), and sulfate radicals ($SO_4^{-\bullet}$).[15] The anode materials are the key factor determining the efficiency of the AO process, which are generally classified into two major categories based on their catalytic performance: active anodes (Pt, RuO_2, IrO_2) and inactive anodes (PbO_2, SnO_2, BDD). The active anodes have low oxygen evolution potential, which promotes the formation of oxides or superoxides on the anode surface, ultimately leading to strong adhesion of $^{\bullet}OH$ species to the electrode surface. Conversely, the inactive anodes exhibit weak $^{\bullet}OH$ adhesion on their surface, allowing the $^{\bullet}OH$ to attack pollutants without selectivity, thereby augmenting the effectiveness of the oxidation.[16] Considering the sufficient amounts of $^{\bullet}OH$ production, inactive anodes are regarded as the most effective anodes in EAOPs processes. However, in inactive anodes, PbO_2 shows poor stability and short service life, and the catalytic oxides (mainly toxic Pb^{2+}) will leach in solution, causing secondary pollution.[17] Similarly, SnO_2 also has the disadvantages of short usage time and insufficient stability, while BDD is limited due to high manufacturing costs.[18] Therefore, developing new anode materials with high catalytic activity, high stability, and environmentally friendly characteristics is the key to promoting the practical application of advanced electrochemical oxidation technology.

Over the past decade, substoichiometric titanium oxides based on Magnéli-phase ceramic electrodes, particularly Ti_4O_7 as an inactive anode, have been studied due to their low cost and high oxidation potential.[19–24] Some research reports indicate that the electro-oxidation activity of Ti_4O_7 is significantly higher than that of active anodes, such as dimensionally stable anode (DSA) or Pt, and can even match the electro-oxidation activity of BDD.[19,21] More importantly, porous reactive electrochemical membrane (REM) utilizing Ti_4O_7 can be fabricated *via* a cost-effective and scalable plasma coating method. When operated in flow-through mode, the REM-based system demonstrates superior current efficiency compared to conventional systems, attributed to the enhanced mass transfer of pollutants from the bulk solution to the anode surface.[25–27] However, previous studies have mainly focused on the removal of tetracycline, amoxicillin, humic acid, *etc.* by the Ti_4O_7 anode, and there is still a lack of systematic research on the removal of sulfonamide antibiotics. Furthermore, most previous studies have only explored a relatively single influencing factor and have not explored the factors that affect Ti_4O_7 REM from multiple perspectives. The optimal operating conditions and degradation mechanism of **SMX** removal by Ti_4O_7 REM are still lacking systematic research. In addition, it is necessary to conduct specific analysis of the toxicity changes of intermediate products and combine them with the ecological environment to ensure the safety of the water body after electrochemical oxidation.

In this study, a flow-through electrochemical filtration system was developed, comprising tubular anodes made of Magnéli-phase Ti_4O_7 and stainless steel (SS) tubular cathodes, for the removal of **SMX**. The effects of current density, initial pH, background electrolyte and humic acid (HA) on the degradation of **SMX** in Ti_4O_7 REM were systematically studied. The degradation pathways of **SMX** were identified by high-performance liquid chromatography coupled with quadrupole time-of-flight tandem mass spectrometry (HPLC-Q-TOF-MS/MS). Furthermore, toxicity analysis during the process was conducted using the Ecological Structure Activity Relationships (ECOSAR) software. This work will provide valuable insights into the electrochemical degradation of refractory organic pollutants in water and wastewater.

2 Materials and methods

2.1. Chemicals

All chemicals are of analytical grade or above and ready for use without the need for further purification. Further details can be found in Text S1 in SI.

2.2. Fabrication and characterization of Ti_4O_7 REM

The fabrication method for Ti_4O_7 REM can be found in Text S2 in SI. The sample morphology of Ti_4O_7 REM was characterized using a Quanta-250 environmental scanning electron microscope (SEM, Phillips/FEI, USA). Crystalline phase analysis was performed with a D8 Advance X-ray diffractometer (XRD, Bruker, USA) employing Cu Kα radiation. Surface chemical composition was determined by X-ray photoelectron spectroscopy (XPS) using an Escalab 250 Xi system (Thermo Fisher Scientific, USA) under high vacuum (1×10^{-9} Torr), with all binding energies referenced to the C 1s peak at 284.8 eV.

2.3. Experimental setup and operation

All electrolysis experiments in the study were conducted in an open 1160 mL cylindrical reactor. In this reactor, Ti_4O_7 REM (diameter of 35 mm, length of 130 mm, effective area of 137 cm^2) served as the anode, and a stainless steel mesh (diameter of 39 mm, length of 130 mm) functioned as the cathode. The anode was positioned centrally within the reactor and encircled by the cathode, maintaining a distance of 2 mm between the electrodes. A direct current (DC) regulated power supply was utilized to supply a constant current intensity. The schematic diagram of the reaction apparatus is shown in Fig. S1. During the experiment, 10 mg L^{-1} **SMX** and a certain concentration of electrolyte were continuously circulated under a peristaltic pump to ensure the solution was thoroughly mixed at room temperature (23 ± 2 °C). The degradation experiment lasted for 120 minutes, and the samples were taken at 0, 5, 15, 30, 45, 60, 80, 100, and 120 minutes. After sampling, the samples were filtered through a mixed fiber membrane with a pore size of 0.22 μm and immediately transferred to a liquid-phase bottle containing 1 mol L^{-1} methanol. The influencing factors of current densities (0.008–0.8 mA cm^{-2}), pH values (3–11), electrolyte concentrations (0.01–0.2 mol L^{-1}), electrolyte types (NaCl, Na_2SO_4 and $NaNO_3$), HA (0–80 mg L^{-1}), and circulation were systematically studied.

2.4. Analytical methods

The analytical methods, including the determination of **SMX** concentration, identification of free radical species, measurement of intermediate products, and toxicity assessment, are detailed in Text S3.

3 Results and discussion

3.1. Characterization and electrochemical properties of Magnéli phase Ti_4O_7 REM

The microstructure of Magnéli-phase titanium oxide can be observed through rutile-type TiO_2 derivatives.[28] During the reorientation process of the TiO_6 octahedral structure, the partial reduction of Ti(IV) to Ti(III) generates defect sites (oxygen vacancies) that lead to the overlap of Ti 3d orbitals within the crystal lattice. This overlap of Ti 3d orbitals is considered to be the reason for the high conductivity of the oxygen-deficient Magnéli-phase.[29] As shown in Fig. 1(a), the SEM image of the Magnéli-phase Ti_4O_7 REM reveals a rough and dense honeycomb-like surface. During high-temperature annealing, the molten nano-TiO_2 powder tends to form Ti_4O_7 aggregates (with diameters ranging from 0.5 to 2.0 μm) during cooling, thus creating abundant pores within the Magnéli-phase Ti_4O_7. This increases the pore volume of the electrode (mesopores and macropores), thereby enhancing the effective contact between organic molecules in the solution and the electrode surface at the electrode/solution interface. The porous microstructure also facilitates flow operations, overcoming the mass transfer limitations (convection) associated with conventional batch electrochemical methods. The XRD pattern of the prepared electrode (Fig. 1(b)) shows major diffraction peaks at 20.7 nm, 26.3 nm, 40.5 nm, *etc.*, consistent with Ti_4O_7.[30] The chemical composition of the Ti_4O_7 REM was further investigated through XPS (Fig. 1(c)). The XPS scanning results indicated the presence of Ti 2p, O 1s, and C 1s on the surface of the Magnéli-phase Ti_4O_7 REM. The C 1s peak is attributed to accidental carbon contamination associated with XPS technology, while the O 1s spectrum can be deconvoluted into three peaks centered at 529.9 eV, 532.6 eV, and 531.2 eV, corresponding to lattice oxygen, surface hydroxyl groups, and oxygen vacancies, respectively. The Ti 2p XPS spectrum (Fig. 1(d)) reveals that both Ti 2p3/2 (458.8 eV) and Ti 2p1/2 (464.4 eV) originate from Ti–O bonding. The binding energy difference between these two characteristic peaks (5.6 eV) suggests that the primary valence state of Ti in the electrode material is +4.[31]

The electrochemical degradation reaction is essentially the transfer of charge between an electronic conductor and an ionic conductor, and the inevitable transformation of biomass or pollutants occurs at the interface between the two phases. This study analyzed the Magnéli-phase Ti_4O_7 REM through electrochemical impedance and as its high-frequency resistance, and the Nyquist spectra of Ti_4O_7 REM are shown in Fig. S2. According to the test fitting results, the internal resistance of the Ti_4O_7 REM is 14.2 Ω, indicating its good conductivity.

3.2. Effect of operational parameters on SMX degradation

3.2.1. Effect of current density. Current density is one of the most crucial factors in the electrochemical oxidation process. It governs the transfer of electrons and the formation of active functional groups, directly influencing the removal rate of organic pollutants. Fig. 2(a) illustrates the relationship between **SMX** variation and electrolysis time under different current densities. Experimental results indicate that the attenuation of **SMX** concentration is related to the applied current density, and as the current density increases, the degradation rate of **SMX** accelerates. This may be attributed to the fact that higher current densities can expedite the indirect electrooxidation rate, namely, the formation rate of ˙OH on the electrode surface.[23] With the extension of electrolysis time, **SMX** can be nearly completely degraded at all current densities, indicating that the Ti_4O_7 electrode has an excellent treatment effect

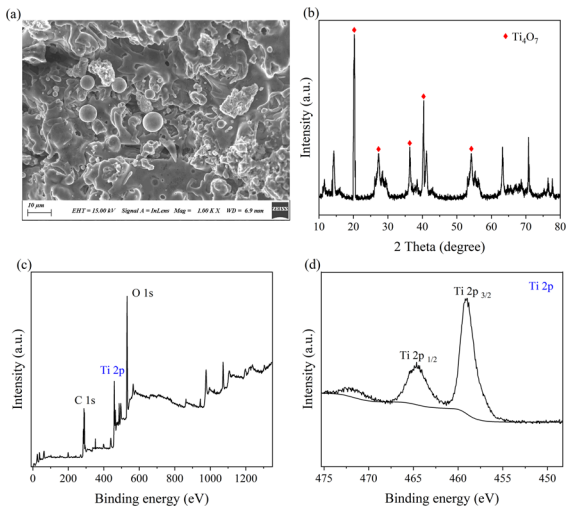

Fig. 1 Characterization of Magnéli-phase Ti_4O_7 REM: (a) SEM image, (b) XRD spectrum, (c) full-spectrum XPS, and (d) Ti 2p XPS spectrum.

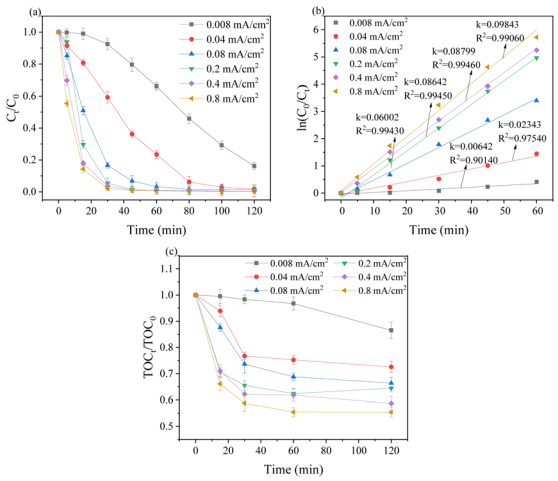

Fig. 2 Effect of current density on SMX degradation (a), quasi-first-order kinetic fitting (b), and TOC removal (c). (Conditions: initial concentration of SMX is 10 mg L^{-1}, electrolyte Na_2SO_4 concentration is 0.1 mol L^{-1}, pH is not adjusted.)

on **SMX**. Through linear regression fitting of experimental data, the kinetic parameters were calculated. As shown in Fig. 2(b), the electrochemical oxidation of **SMX** conforms to a pseudo-first-order kinetic reaction, and there is a good linear correlation between removal efficiency and electrolysis time. The apparent rate constant k can be obtained by analyzing the slope of the curve. It can be found that the value of k increases with the increase in current density. As the current density increases from 0.008 mA cm^{-2} to 0.8 mA cm^{-2}, the values of k vary from 0.00642 to 0.09843. Furthermore, Fig. 2(c) shows the effect of current density on the removal of TOC. It can be observed that the TOC removal rate increases with the increase of applied current density and electrolysis time. However, when the current density reaches its maximum value (0.8 mA cm^{-2}), the TOC removal rate is only 46.23%, indicating that **SMX** was not completely mineralized by Ti_4O_7 REM. In addition, the energy consumption of the electrode during the electrocatalytic oxidation process was also calculated according to eqn (S3) in the SI. As listed in Table S1, when the current density reaches 0.08 mA cm^{-2}, the degradation rate of **SMX** can reach over 99% within 2 hours. Combined with the voltage drift under different current density states during the experimental process, the calculated energy consumption is only 9.89 kWh kg^{-1} TOC, which is much lower than the 57.63 kWh kg^{-1} TOC at 0.8 mA cm^{-2}. It can be found that when the removal rates are similar, the energy consumption continues to increase with the increase of current density. Therefore, to reduce energy consumption, 0.08 mA cm^{-2} is selected as the optimal current density in this study. Moreover, Table S2 compares the energy consumption of similar electrochemical systems for removing target pollutants, providing a benchmark for the energy consumption of such electrochemical systems. From Table S2, we can see that the energy consumption of this study is lower than that of most similar electrochemical oxidation systems. Therefore, we believe that the current density selected for this experiment is relatively low-energy, environmentally friendly, and efficient.

3.2.2. Effect of initial pH. The pH value is widely believed to significantly affect the effectiveness of the electrochemical oxidation process.[23,32] Therefore, the effect of initial pH (pH = 3, 7, and 11) on **SMX** degradation was investigated in this experiment, with a current density set at 0.08 mA cm^{-2}. As shown in Fig. 3(a), the final degradation effects of **SMX** under pH = 3 and pH = 7 conditions are similar, and much better than that under pH = 11. However, according to quasi-first-order kinetic fitting in Fig. 3(b), it can be observed that the k value reaches a maximum of 0.04830 at pH = 7. Similarly, Fig. 3(c) shows that the TOC removal at pH = 7 is higher than that at pH = 3 and 11. It has been reported that the structure of **SMX** can also affect the degradation process under different pH conditions.[33,34] The pK_a values of **SMX** are 1.8 (pK_{a_1}) and 5.5 (pK_{a_2}). When pH < pK_{a_1}, the protonated structure of **SMX** renders it positively charged, preventing the delocalization of unshared electron pairs from the N atom to the aromatic ring, thereby reducing its reactivity with electrophilic radicals. When pH > pK_{a_2}, the radical oxidation activity of the aniline group is enhanced due to the deprotonation of the –NH sulfonamide group. Therefore, when pH = 7, the free radical oxidation activity of the aniline group in **SMX** is strong, so the removal rate is the highest under this condition. Ultimately, pH = 7 was chosen as the optimal reaction condition in this study.

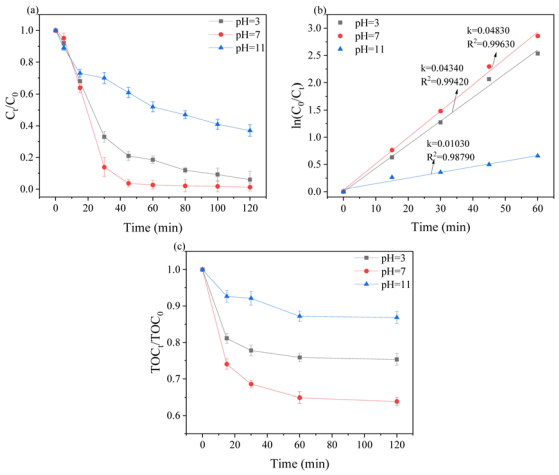

Fig. 3 Effect of pH on SMX degradation (a), quasi-first-order kinetic fitting (b), and TOC removal (c). (Conditions: initial concentration of SMX is 10 mg L^{-1}, electrolyte Na_2SO_4 concentration is 0.1 mol L^{-1}, current density is 0.08 mA cm^{-2})

3.2.3. Effect of electrolyte concentration. In addition to current density, electrolyte concentration is also a factor affecting electrochemical oxidation. Therefore, the effect of Na_2SO_4 concentrations on **SMX** removal was studied. Among them, the concentration range of Na_2SO_4 solution was from 0.01 mol L^{-1} to 0.2 mol L^{-1}, the initial concentration of **SMX** was 10 mg L^{-1}, the current density was 0.08 mA cm^{-2}, and the pH was 7. As depicted in Fig. 4(a) and (b), when the electrolyte concentration was 0.01, 0.05, 0.1, and 0.2 mol L^{-1}, **SMX** was almost completely removed within 2 hours, and the k values showed an upward trend, which were 0.04730, 0.05830, 0.06470,

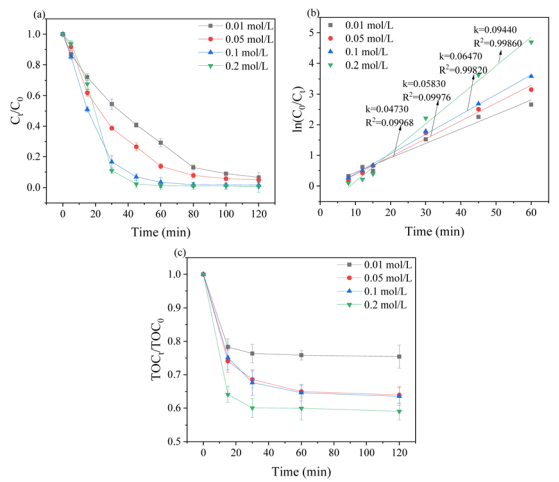

Fig. 4 Effect of electrolyte concentration on SMX degradation (a), quasi-first-order kinetic fitting (b) and TOC removal (c). (Conditions: initial concentration of SMX is 10 mg L^{-1}, current density is 0.08 mA cm^{-2}, pH = 7.)

and 0.09440, respectively. Besides, it can be observed in Fig. 4(c) that as the electrolyte concentration increased, the removal rate of TOC also increased. The above results indicate that as the electrolyte concentration increases, the degradation rate of **SMX** accelerates. This may be mainly due to the enhancement of **SMX** mass transfer rate in the system under higher ionic strength, thus accelerating the observed degradation kinetics. The reduction in ohmic losses might be another reason for the accelerated degradation rate of **SMX**. However, the current density of the reaction condition in this experiment is fixed at 0.08 mA cm^{-2}. Under this condition, the effect of changing electrolyte concentration on ohmic loss may be minor. The above result is similar to the previous study,[35] which enhanced the mass transfer of target pollutants through electrolytes. However, it is worth noting that when the Na_2SO_4 concentration continues to increase after 0.1 mol L^{-1}, the degradation of **SMX** increases very slowly. This is because there is a critical electrolyte concentration in each electrolysis system. When the concentration is below this critical concentration, the system lacks sufficient ions to conduct current, thereby reducing oxidation efficiency. Above the critical electrolyte concentration, when the electrolyte concentration is low, the conductive ions in the solution are nearly saturated. Therefore, increasing the electrolyte concentration barely enhances electrolysis efficiency. Considering both the critical electrolyte concentration and the cost-effectiveness of the experiment, it was ultimately decided to use 0.1 mol L^{-1} Na_2SO_4 as the optimal electrolyte concentration.

3.2.4. Effect of electrolyte types. The supporting electrolyte can generate oxidizing species and react with organic pollutants in the solution, which will have a great impact on the oxidation ability of this experimental system. In this study, 0.1 mol L^{-1} Na_2SO_4, NaCl and $NaNO_3$ were selected as supporting electrolytes, and their effects were compared under the conditions of current density of 0.08 mA cm^{-2} and pH value of 7. As shown in Fig. 5(a), the removal rate of **SMX** is the highest when Na_2SO_4 is used as the background electrolyte, reaching 99.7%. Meanwhile, Fig. 5(b) and (c) also show that the removal rate of quasi-first-order kinetic fitting and TOC is the best when Na_2SO_4 is used as the background electrolyte. In addition, we also compared the energy consumption and voltage drift in the process of removing **SMX** with three different supporting electrolytes (Table S3). The results showed that when NaCl and $NaNO_3$ were used as electrolyte, the energy consumption of electrolyte was much greater than that when Na_2SO_4 was used as electrolyte, which was similar to previous studies.[36]

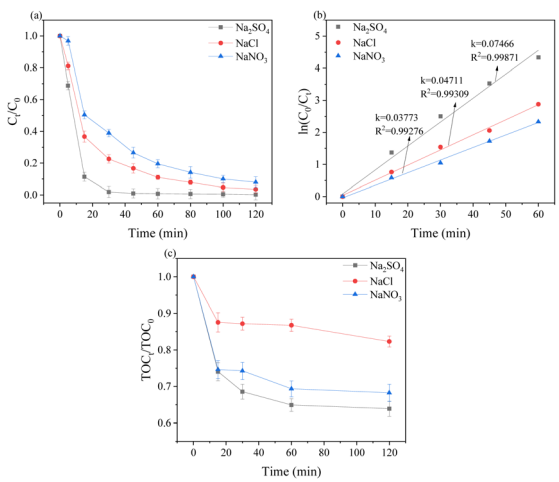

Fig. 5 Effect of electrolyte type on SMX degradation (a), quasi-first-order kinetic fitting (b), and TOC removal (c). (Conditions: initial concentration of SMX is 10 mg L^{-1}, current density is 0.08 mA cm^{-2}, pH = 7, electrolytes Na_2SO_4, NaCl and $NaNO_3$ are all 0.1 mol L^{-1})

The observed efficient degradation of **SMX** under Na_2SO_4 supporting electrolyte could be attributed to the following factors. According to previous studies, when Na_2SO_4 was used as the supporting electrolyte, $S_2O_8^{2-}$ may be generated at the inactive anode, as listed in eqn (1).[37] $S_2O_8^{2-}$ is a strong oxidizer, with a standard redox potential E_0 of +2.01 V, which is close to that of ozone (E_0 = +1.70 V) and higher than that of permanganate (E_0 = +1.51 V), thus possessing a strong ability to oxidatively degrade organic pollutants.[38] Then, according to the previous study,[39] it would be reduced at the cathode (eqn (2)). The E_0 value of $SO_4^{-\bullet}$ is 2.5–3.1 V, exceeding the E_0 value of $^{\bullet}OH$ (E_0 = 1.9–2.7 V),[40] and its half-life is longer than that of $^{\bullet}OH$, indicating better stability. It can travel a longer distance during the reaction time, which is more conducive to the oxidative degradation of organic pollutants.[41,42]

$$2SO_4^{2-} \rightarrow S_2O_8^{2-} + 2e^- \quad (1)$$

$$S_2O_8^{2-} + e^- \rightarrow SO_4^{-\bullet} + SO_4^{2-} \quad (2)$$

When NaCl is used as the electrolyte, ClO^- can be generated through the reaction of Cl^- and OH^- (eqn (3)). ClO^- is a strong oxidant with a standard redox potential E_0 of +1.67 V, thus can effectively promote **SMX** degradation.[43] However, as illustrated in eqn (4), the presence of Cl^- may lead to competitive reactions by scavenging $^{\bullet}OH$ generated in the electrolyte through radical chain transfer reactions, leading to poor **SMX** removal efficiency under the NaCl supporting electrolyte.

$$Cl^- + OH^- \rightarrow ClO^- + H_2O + 2e^- \quad (3)$$

$$Cl^- + {}^{\bullet}OH \rightarrow Cl^{\bullet} + OH^- \quad (4)$$

When $NaNO_3$ was used as the electrolyte, the anodic reactions in eqn (5)–(8) occurred. These substances, particularly NH_3, can react with $^{\bullet}OH$,[44] leading to a decrease in **SMX** degradation. Based on comprehensive experimental results, 0.1 mol L^{-1} Na_2SO_4 was selected as the optimal electrolyte type for the reaction system.

$$NO_3^- + 6H_2O + 8e^- \rightarrow NH_3 + 9OH^- \quad (5)$$

$$NO_3^- + 2H^+ + 2e^- \rightarrow NO_2^- + H_2O \quad (6)$$

$$NO_2^- + 5H_2O + 6e^- \rightarrow NH_3 + 7OH^- \quad (7)$$

$$2NH_3 + 6{}^{\bullet}OH \rightarrow N_2 + 6H_2O \quad (8)$$

3.2.5. Effect of HA. Natural organic matter (NOM) is widely distributed in surface water and has a significant impact on the degradation of antibiotics in electrochemical oxidation systems. This study used HA as a typical NOM and investigated its effect on the degradation of **SMX** in the Magnéli-phase Ti_4O_7 system at concentrations of 0, 10, 20, 40, and 80 mg L^{-1}. As shown in Fig. 6(a), the addition of HA inhibited the electrochemical degradation of **SMX**. After 2 hours of electrolysis, **SMX** was completely removed without the presence of HA. However, under the same experimental conditions, when HA is present, residual **SMX** was detected in the solution after the reaction was completed. Furthermore, as shown in Fig. 6(b), with the addition of HA, the k value decreased from 0.06000 to 0.02665, indicating that the presence of HA can react with $^{\cdot}OH$ and inhibit the degradation of **SMX**. On the one hand, HA may complex with antibiotics, and its significant steric hindrance can affect the migration of antibiotics. On the other hand, HA will compete with antibiotics and mineralize on the anode surface.[45] Based on the analysis of the experimental results, 0 mg L^{-1} HA was ultimately selected as the optimal reaction condition.

3.2.6. Effect of circulation. To verify the effect of flow-through mode on electrochemical oxidation, the removal of **SMX** under cycle and no cycle conditions was compared, based on the optimal reaction conditions. As shown in Fig. S3, the removal efficiency of **SMX** in the cycle condition is significantly higher than that in the no cycle condition. This is mainly because the reaction solution circulates under the suction of the peristaltic pump. During the circulation process, dissolved oxygen is converted into $^{\cdot}OH$ through the action of the cathode, and then injected into the Ti_4O_7 electrode. At this time, $^{\cdot}OH$ is electrostatically attracted by the anode, which accelerates the mass transfer rate at the interface.

3.3. Intermediate products and degradation pathways of SMX

3.3.1. Identification of key substances. The free radicals generated on the anode surface are considered to be the main oxidant for pollutant degradation in EAOPs. As shown in Fig. 7(a), two obvious EPR signals of DMPO-$^{\cdot}OH$ adduct and DMPO-$SO_4^{-\cdot}$ adduct were detected in the Ti_4O_7 REM system.[46]

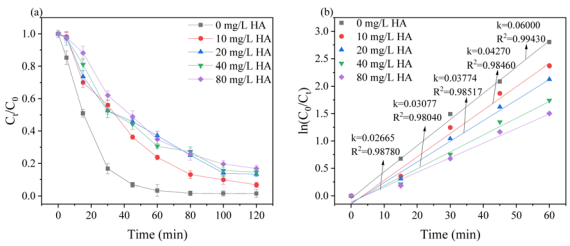

Fig. 6 Effect of HA on SMX degradation (a) and quasi-first-order kinetic fitting (b). (Conditions: initial concentration of SMX is 10 mg L^{-1}, electrolyte Na_2SO_4 concentration is 0.1 mol L^{-1}, current density is 0.08 mA cm^{-2}, pH = 7.)

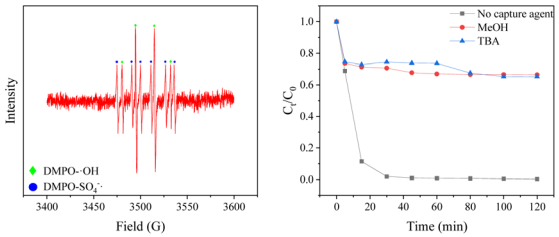

Fig. 7 EPR spectrum of DMPO capturing $^{\cdot}OH$ and $SO_4^{-\cdot}$ at 15 minutes (a) and effects of different trapping agents on SMX degradation (b). (Conditions: initial concentration of SMX is 10 mg L^{-1}, electrolyte Na_2SO_4 concentration is 0.1 mol L^{-1}, concentrations of MeOH and TBA are 0.1 mol L^{-1}, current density is 0.08 mA cm^{-2}, pH = 7.)

$^{\cdot}OH$ has a high standard redox potential (E_0 = 1.9–2.7 V) and can mineralize organic pollutants non selectively. The formation of $^{\cdot}OH$ in the system can be explained by eqn (9).[47] $SO_4^{-\cdot}$ is a strong oxidant with a redox potential of 2.5–3.1 V. Previous studies have shown that $SO_4^{-\cdot}$ (eqn (10)) can be formed by sulfate oxidation on inactive anode,[48] and the specific generation process of $SO_4^{-\cdot}$ has been introduced in 3.2.4.

$$Ti_4O_7 + H_2O \rightarrow Ti_4O_7(^{\cdot}OH) + H^+ + e^- \quad (9)$$

$$SO_4^{2-} \rightarrow SO_4^{-\cdot} + e^- \quad (10)$$

In order to further explore the free radicals that play a major role in this study, quenching experiments was conducted. *Tert*-Butanol (TBA) and methanol (MeOH) were selected as the free radical trapping agents. The reaction rate constant of TBA with $^{\cdot}OH$ is 2.8×10^9 M^{-1} s^{-1},[49] which can quickly capture the $^{\cdot}OH$ generated on the electrode surface, and no other radicals are generated during the reaction pathway. MeOH can serve as an effective scavenger for both $^{\cdot}OH$ ($k = 9.7 \times 10^8$ M^{-1} s^{-1}) and $SO_4^{-\cdot}$ ($k = 1.1 \times 10^7$ M^{-1} s^{-1}) radicals.[50] Therefore, to investigate the active species playing a major role in the electro-oxidation reaction, 0.1 mol L^{-1} MeOH and 0.1 mol L^{-1} TBA were added to the **SMX** electrocatalytic oxidation degradation process for capture experiments. The contributions of the two capture agents to the two types of radicals were explored and quantitatively analyzed. As can be seen from Fig. 7(b), when TBA is added to the electrochemical system, the $^{\cdot}OH$ generated by electrocatalytic oxidation is largely captured, resulting in a sharp decrease in the removal rate of **SMX** from 99.3% to 30.2%. Similarly, in the presence of MeOH, both $^{\cdot}OH$ and $SO_4^{-\cdot}$ generated in the system are captured and removed, significantly inhibiting the electrocatalytic activity of the system. However, there is no significant difference in the impact of the two scavengers on the removal of **SMX** in the electrochemical system, indicating that $SO_4^{-\cdot}$ is not the main active species in the system, while $^{\cdot}OH$ plays a dominant role in the electro-oxidative degradation of **SMX**.

3.3.2. Degradation pathway. Based on the analytical results of intermediates derived from mass spectrometry, the electrochemical oxidative degradation pathway of **SMX** in the Magnéli-phase Ti_4O_7 system was proposed, as illustrated in Fig. 8. The mass-to-charge ratios (m/z), molecular formulas, and potential

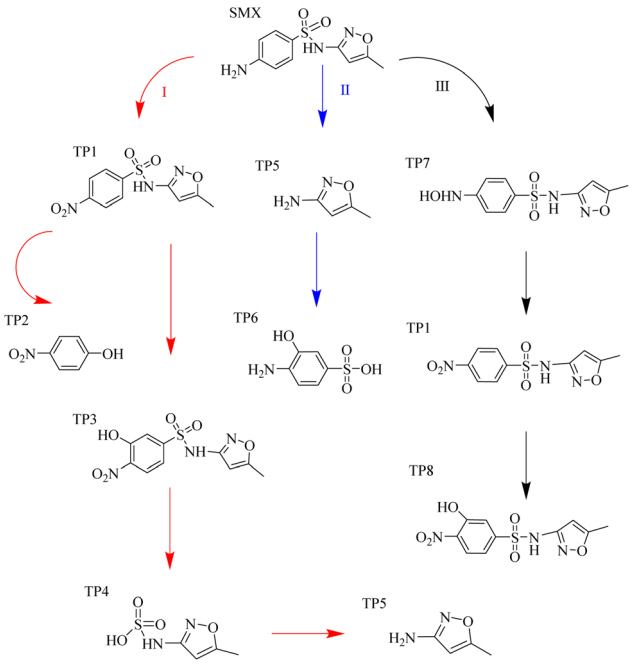

Fig. 8 Possible electrocatalytic degradation pathways of SMX in the Magnéli-phase Ti_4O_7 system.

structures of the intermediate products can be accessed in Table S4 in the SI. Overall, the degradation of **SMX** can primarily be categorized into the following three pathways.

In pathway I, the primary reaction is the oxidation of amine groups, resulting in the formation of nitro-**SMX** derivatives.[51] Amino is oxidized by ˙OH to produce a nitro-**SMX** derivative. This may be due to rapid and reversible hydration, which leads to the formation of an aniline radical at the N-center. The aniline radical is further neutralized by molecular oxygen, resulting in the hydrolysis of hydroxylamine and nitroso derivatives into nitro-**SMX.**[52] Afterwards, ˙OH attacks the benzene ring, generating **TP2** and **TP4**. Through the continuous hydroxylation of these primary by-products, **SMX** can ultimately be mineralized into CO_2, H_2O, SO_4^{2-}, and NO_3^-. These reaction pathways are consistent with previous studies on **SMX** degradation.[34,53] In pathway II, the S–N bond serves as the electron-rich site of **SMX**, which is attacked by ˙OH, leading to the breakage of the sulfonamide bond to generate **TP5.**[54] The ˙OH can further attack the isoxazole ring to produce the ring-opening product **TP6**, which is similar to previous studies.[37] In pathway III, the $-NH_2$ group on **SMX** aniline undergoes hydroxylation, leading to the formation of **TP7** and intermediate product **TP1**, and is further transformed into **TP8**.

3.4. Toxicity analysis

Due to the generation of numerous intermediate products during the electrolysis process, it is imperative to assess the potential environmental risks posed by these products. The acute and chronic toxicity of **SMX** and its intermediate products to daphnia, green algae, and fish is estimated based on the globally harmonized system (GHS) of classification and labelling of chemicals. According to the GHS, toxicity data is categorized into four levels, namely highly toxic (LC 50/EC 50/ChV $\leq$ 1 mg L^{-1}), toxic (1 mg L^{-1} < LC 50/EC 50/ChV $\leq$ 10 mg L^{-1}), harmful (10 mg L^{-1} < LC 50/EC 50/ChV $\leq$ 100 mg L^{-1}), and harmless (LC 50/EC 50/ChV > 100 mg L^{-1}).[55,56] The results predicted by the ECOSAR program are presented in Table 1. The results demonstrated that **SMX** exhibits varying levels of toxicity towards the aforementioned organisms. Daphnia magna is also the most sensitive organism to **SMX** and its by-products. The toxicity of the degradation end-products of **SMX** shows a decreasing trend, except for the intermediate product **TP5**, whose toxicity decreases. We can also observe that the toxicity of the final products **TP4**, **TP6** and **TP8** is significantly lower than that of **SMX**. Among them, we can observe that each index of **TP4** after treatment has reached a harmless state; **TP6** only had high chronic toxicity to Daphnia, and other toxicities were reduced. **TP8** has slight toxicity to Fish Daphnia Green, and other toxicity has also been well controlled. More importantly, the significant reduction in toxicity level (from high toxicity to low toxicity/non toxicity) indicates that Ti_4O_7 REM not only

Table 1 Predicted toxicity of SMX and its TPs by ECOSAR program

Compounds	Acute toxicity (mg L^{-1})			Chronic toxicity (mg L^{-1})		
	Fish (96 h-LC_{50})	Daphnia (48 h-LC_{50})	Green algae (96 h-LC_{50})	Fish (ChV)	Daphnia (ChV)	Green algae (ChV)
SMX	267	6.43	21.8	5	0.068	11.1
TP1	1170	619	342	105	49.3	76.2
TP2	1145	556	325	98.2	46.3	73.7
TP3	1010	539	309	91.7	44.1	70.4
TP4	8650	3010	2950	4740	7490	2590
TP5	270	3.63	13.8	6.59	0.0369	9.16
TP6	1940	291	1670	1270	2.31	3010
TP7	5550	2730	1120	458	178	213
TP8	1010	539	309	91.7	44.1	70.4

Highly toxic Toxic Harmful Harmless

destroys the target pollutant structurally, but also realizes a key environmental detoxification process. This ability to convert high environmental risk parent compounds into low environmental risk conversion products is one of the core indicators to evaluate whether advanced oxidation technology can be safely applied. The toxicity of the final product is far below the threshold of chronic damage to sensitive aquatic organisms at the population level. Therefore, the Magnéli-phase Ti_4O_7 system reduces the overall toxicity of **SMX** and has great potential in protecting aquatic ecosystems.

4 Conclusions

In this study, a stable and effective electrochemical filtration system using Magnéli-phase Ti_4O_7 REM was successfully established for the removal of **SMX** from water. The effect of current density, pH, electrolyte concentration and types, HA, and circulation on **SMX** degradation was systematically investigated. The results indicate that the degradation of **SMX** follows first-order reaction kinetics. Within the current density range of 0.008–0.8 mA cm^{-2}, the degradation rate of **SMX** increases with increasing current density. The optimal parameters for **SMX** degradation by Ti_4O_7 are under cyclic conditions, current density is 0.08 mA cm^{-2}, electrolyte is 0.1 mol L^{-1} Na_2SO_4, pH = 7, and no HA. Under this condition, the removal efficiency of **SMX** reaches over 99.7%, which depends on the $^{\bullet}OH$ generated at the anode, indicating that this technology has good electro-oxidation efficiency. It is inferred that the degradation pathway of **SMX** can be divided into three types: oxidation of the amino group by $^{\bullet}OH$, breakage of the S–N bond, and hydroxylation of $-NH_2$. Meanwhile, a toxicity evaluation of the **SMX** degradation process was conducted, and the results showed that the overall toxicity decreased after 2 hours of **SMX** treatment. In summary, the Magnéli-phase Ti_4O_7 REM may provide a new effective strategy for the removal of refractory organic pollutants in water and wastewater.

Author contributions

Qiang Liu: methodology, validation. Yinuo Wang: formal analysis, writing-original draft, writing-review & editing. Boxuan Yang: methodology, figure supplementation and test polishing. Jinwei Li: conceptualization. Chengchun Jiang: visualization, supervision. Huan Wang: investigation.

Conflicts of interest

The authors declare that there are no conflicts of interest.

Data availability

The data supporting the findings of this study are available from the corresponding author upon reasonable request.

Supplementary information (SI) is available. See DOI: **https://doi.org/10.1039/d5ra06264k**.

Acknowledgements

This work is supported by Shenzhen Science and Technology Program (RCBS20231211090623038), the National Natural Science Foundation of China (No. 52170007), Shenzhen Polytechnic University Research Fund (6023310040K), and Natural Science Foundation of Guangdong Province of China (No. 2023A1515012063).

Notes and references

1 R. Meffe and I. de Bustamante, *Sci. Total Environ.*, 2014, **481**, 280–295.
2 I. Ali, A. Barros de Souza, S. De Laet, K. Van Eyck and R. Dewil, *Chemosphere*, 2023, **319**, 137984.
3 W. Yang, H. Dong, Y. Tian, Y. Tong, J. Lu, L. Liao and J. Niu, *Sep. Purif. Technol.*, 2025, **357**, 130044.
4 S. N. Misal, M.-H. Lin, S. Mehraeen and B. P. Chaplin, *J. Hazard. Mater.*, 2020, **384**, 121420.
5 S. D. Richardson, M. J. Plewa, E. D. Wagner, R. Schoeny and D. M. DeMarini, *Mutat. Res., Rev. Mutat. Res.*, 2007, **636**, 178–242.
6 S. Gao, Z. Zhao, Y. Xu, J. Tian, H. Qi, W. Lin and F. Cui, *J. Hazard. Mater.*, 2014, **274**, 258–269.
7 F. J. Beltrán, A. Aguinaco, J. F. García-Araya and A. Oropesa, *Water Res.*, 2008, **42**, 3799–3808.
8 R. F. Dantas, S. Contreras, C. Sans and S. Esplugas, *J. Hazard. Mater.*, 2008, **150**, 790–794.
9 A. G. Gonçalves, J. J. M. Órfão and M. F. R. Pereira, *J. Hazard. Mater.*, 2012, **239–240**, 167–174.
10 A. G. Trovó, R. F. P. Nogueira, A. Agüera, C. Sirtori and A. R. Fernández-Alba, *Chemosphere*, 2009, **77**, 1292–1298.
11 A. J. Watkinson, E. J. Murby and S. D. Costanzo, *Water Res.*, 2007, **41**, 4164–4176.
12 K. P. de Amorim, L. L. Romualdo and L. S. Andrade, *Sep. Purif. Technol.*, 2013, **120**, 319–327.
13 A. Fabiańska, A. Białk-Bielińska, P. Stepnowski, S. Stolte and E. M. Siedlecka, *J. Hazard. Mater.*, 2014, **280**, 579–587.
14 N. Oturan, S. O. Ganiyu, S. Raffy and M. A. Oturan, *Appl. Catal., B*, 2017, **217**, 214–223.
15 R. Fu, P.-S. Zhang, Y.-X. Jiang, L. Sun and X.-H. Sun, *Chemosphere*, 2023, **311**, 136993.
16 C. A. Martínez-Huitle and M. Panizza, *Curr. Opin. Electrochem.*, 2018, **11**, 62–71.
17 Y. Zhang, P. He, L. Zhou, F. Dong, D. Yang, H. Lei, L. Du, L. Jia and S. Zhou, *Ecotoxicol. Environ. Saf.*, 2020, **188**, 109921.
18 W. Wu, Z.-H. Huang and T.-T. Lim, *J. Environ. Chem. Eng.*, 2016, **4**, 2807–2815.
19 H. Olvera-Vargas, J.-C. Rouch, C. Coetsier, M. Cretin and C. Causserand, *Sep. Purif. Technol.*, 2018, **203**, 143–151.
20 S. O. Ganiyu, N. Oturan, S. Raffy, M. Cretin, C. Causserand and M. A. Oturan, *Sep. Purif. Technol.*, 2019, **208**, 142–152.
21 S. O. Ganiyu, N. Oturan, S. Raffy, G. Esposito, E. D. van Hullebusch, M. Cretin and M. A. Oturan, *Electrochim. Acta*, 2017, **242**, 344–354.

22 T. Maqbool, Q. V. Ly, K. He, L. Cui, Y. Zhang, M. Sun and Z. Zhang, *J. Membr. Sci.*, 2022, **651**, 120460.
23 W. Yang, N. Oturan, S. Raffy, M. Zhou and M. A. Oturan, *Chem. Eng. J.*, 2020, **383**, 123155.
24 Y. Zhang, J. Ding, Q. Gao, B. Jiang, C. Li and Q. Zhao, *Process Saf. Environ. Prot.*, 2022, **159**, 931–943.
25 H. Lin, H. Peng, X. Feng, X. Li, J. Zhao, K. Yang, J. Liao, D. Cheng, X. Liu, S. Lv, J. Xu and Q. Huang, *Water Res.*, 2021, **190**, 116790.
26 S. O. Ganiyu, N. Oturan, S. Raffy, M. Cretin, R. Esmilaire, E. van Hullebusch, G. Esposito and M. A. Oturan, *Water Res.*, 2016, **106**, 171–182.
27 C. Trellu, M. Rivallin, S. Cerneaux, C. Coetsier, C. Causserand, M. A. Oturan and M. Cretin, *Chem. Eng. J.*, 2020, **400**, 125936.
28 A. F. Arif, R. Balgis, T. Ogi, F. Iskandar, A. Kinoshita, K. Nakamura and K. Okuyama, *Sci. Rep.*, 2017, **7**, 3646.
29 C.-H. Lee, Y.-K. Lim, E.-S. Lee, H.-J. Lee, H.-D. Park and D.-S. Lim, *RSC Adv.*, 2018, **8**, 11102–11108.
30 S. Liang, H. Lin, X. Yan and Q. Huang, *Chem. Eng. J.*, 2018, **332**, 628–636.
31 M. P. Casaletto, G. M. Ingo, S. Kaciulis, G. Mattogno, L. Pandolfi and G. Scavia, *Appl. Surf. Sci.*, 2001, **172**, 167–177.
32 F. Li, X. Peng, Y. Liu, J. Mei, L. Sun, C. Shen, C. Ma, M. Huang, Z. Wang and W. Sand, *Chemosphere*, 2019, **229**, 383–391.
33 Y. Fan, Y. Ji, D. Kong, J. Lu and Q. Zhou, *J. Hazard. Mater.*, 2015, **300**, 39–47.
34 H. Lin, J. Niu, J. Xu, Y. Li and Y. Pan, *Electrochim. Acta*, 2013, **97**, 167–174.
35 H. Yun, C. Lim, M. Kwon, D. Lee, Y. Yun, D.-H. Seo and K. Yong, *Adv. Mater.*, 2024, **36**, 2408280.
36 P. Saha, J. Wang, Y. Zhou, L. Carlucci, A. W. Jeremiasse, H. H. M. Rijnaarts and H. Bruning, *Environ. Res.*, 2022, **211**, 113057.
37 H. Hai, X. Xing, S. Li, S. Xia and J. Xia, *Sci. Total Environ.*, 2020, **738**, 139909.
38 C. Liang, C. Yi-Chi and Y.-L. Lin, *Soil Sediment Contam.: Int. J.*, 2012, **21**, 701–719.
39 J. Liu, S. Zhong, Y. Song, B. Wang and F. Zhang, *J. Electroanal. Chem.*, 2018, **809**, 74–79.
40 X. Chen, M. Murugananthan and Y. Zhang, *Chem. Eng. J.*, 2016, **283**, 1357–1365.
41 A. Rastogi, S. R. Al-Abed and D. D. Dionysiou, *Appl. Catal., B*, 2009, **85**, 171–179.
42 C. Liang, C.-F. Huang and Y.-J. Chen, *Water Res.*, 2008, **42**, 4091–4100.
43 P. Britto-Costa and L. Ruotolo, *Braz. J. Chem. Eng.*, 2012, **29**, 763–773.
44 C. Wang, L. Yin, Z. Xu, J. Niu and L.-A. Hou, *Chem. Eng. J.*, 2017, **326**, 911–920.
45 C. Trellu, Y. Péchaud, N. Oturan, E. Mousset, D. Huguenot, E. D. van Hullebusch, G. Esposito and M. A. Oturan, *Appl. Catal., B*, 2016, **194**, 32–41.
46 Y. Gao, Q. Yue, B. Gao and A. Li, *Sci. Total Environ.*, 2020, **746**, 141094.
47 J. Wang and R. Zhuan, *Sci. Total Environ.*, 2020, **701**, 135023.
48 Y. Yao, C. Huang, Y. Yang, M. Li and B. Ren, *Chem. Eng. J.*, 2018, **350**, 960–970.
49 G. V. Buxton, C. L. Greenstock, W. P. Helman and A. B. Ross, *J. Phys. Chem. Ref. Data*, 1988, **17**, 513–886.
50 P. Xie, J. Ma, W. Liu, J. Zou, S. Yue, X. Li, M. R. Wiesner and J. Fang, *Water Res.*, 2015, **69**, 223–233.
51 S. Wang and J. Wang, *Chem. Eng. J.*, 2018, **351**, 688–696.
52 S. Wang, W. Xu, J. Wu, Q. Gong and P. Xie, *Sep. Purif. Technol.*, 2020, **235**, 116170.
53 S. Feng, J. Lin, S. Sun and F. Zhang, *Chin. J. Oceanol. Limnol.*, 2017, **35**, 153–162.
54 S. Zeb, S. Hussain, H. A. Khan, Z. Ali, N. Khan, K. I. Khan, F. Ali, S. khan, M. del Pilar Taboada Sotomayor and S. Gul, *Int. J. Electrochem. Sci.*, 2018, **13**, 9428–9440.
55 X. Ao, W. Liu, W. Sun, C. Yang, Z. Lu and C. Li, *Chemosphere*, 2018, **212**, 365–375.
56 K. S. Tay and N. Madehi, *Sci. Total Environ.*, 2015, **520**, 23–31.